Chaos, Solitons & Fractals Vol. 1, No. 6, pp.511–528, 1991
Printed in Great Britain

Dynamics of Maps with a Global Multiplicative Coupling

R. LÓPEZ-RUIZ and C. PÉREZ-GARCÍA*

Departamento de Física y Matemática Aplicada, Facultad de Ciencias, Universidad de Navarra, E-31080 Pamplona (Navarra), Spain

Abstract—The dynamics of coupled logistic maps with a multiplicative coupling is analyzed. We determine the transition to chaos and the multifractal properties of some of the attractors studied in the particular case of only two coupled maps. This transition cannot be deduced from the subharmonic cascade typical of a single map. The results are generalized to an ensemble of globally coupled maps with a similar multiplicative coupling. The global quantities have different attractors depending on the coupling strength and the number of elements in the ensemble.

1. INTRODUCTION

Extended systems far from equilibrium can change from almost regular patterns to strong turbulence when some pumping parameter is changed. Near a critical threshold the dynamics are dominated by few relevant modes. By increasing a control parameter the system becomes irregular. These irregular motions are due to the interplay of many unstable modes that act on a extended system in different places as observed in many physical situations [1].

Some efforts to understand the irregular behavior of extended systems have been made in recent years. Some ideas have been tested by using some models that 'mimic' complex behavior [2]. Cellular automata (CA) [3], for example, have simple dynamics given by a deterministic rule that leads to an unpredictable behavior in many cases. Another class of very interesting dynamical systems currently under study are coupled map lattices (CML), that obey to a simple deterministic equations (discrete in time) with a diffusive coupling [4, 5].

$$x_{n+1}^{i} = (1-\varepsilon)f(x_n^i) + \frac{1}{2}\varepsilon[f(x_n^{i+1}) + f(x_n^{i-1})] \tag{1}$$

where ε is similar to a diffusion coefficient. They show some qualitative similarities (spatio-temporal intermittency) with experiments.

However, many physical and biological situations seem to be due to a complex connectivity among complex elements. Therefore, a feedback (not merely diffusive) mechanism between the single component and the ensemble seems to be another suitable way to understand complexity. Moreover, in some experiments (on turbulence, for example) only global properties, i.e. averages of contributions of many components, are accessible to measurements. This is the case, for example, of the electrocardiogram or the

* Also at the Departament de Física, Universitat Autònoma de Barcelona, E-08193 Bellaterra (Catalonia), Spain.

electroencephalogram, whose complex dynamics are a result of the average over many complex elements.

Following these ideas, Kaneko has proposed an extension of the previously studied CML, to a kind of global coupled maps (GCM) in the form [6]

$$x^i_{n+1} = (1 - \varepsilon)f(x^i_n) + \frac{\varepsilon}{N}\sum_{j=1}^{N} f(x^j_n). \tag{2}$$

These (GCM) may be seen as an extreme limit of long-range coupling that resembles a mean-field theory for maps. Of course, such extended models are far too simple to reproduce the properties of given systems. Nevertheless, some simulations indicate that formations of 'phases', and jumps between different attractors are possible in these simple systems [6].

We propose to analyze the consequences of a different global coupling among the maps. Here a feedback through the 'growth rate', i.e. the control parameter of the system is considered. This results in a multiplicative global coupling among the maps. The main aim of the present paper is to study in some detail the dynamics of maps linked with such a global multiplicative coupling. In Section 2 we analyze the case of two coupled logistic maps, characterizing their stability and attractors. Section 3 is devoted to study the chaotic zones in the parameter space of these models. In Section 4 we study a multiplicative coupling among these maps, and the different behavior of the average, depending on the the coupling coefficient and the number of coupled maps. The last section contains a discussion and conclusion.

2. DYNAMICS OF TWO MAPS WITH A MULTIPLICATIVE COUPLING

2.1. *Models*

We begin by considering multiplicative coupling between two maps. The logistic map is taken because it has a well-known route to the turbulence. Hence, the system considered is a 2-dimensional extension of the logistic map

$$x_{n+1} = \mu x_n(1 - x_n) \qquad y_{n+1} = \mu' y_n(1 - y_n) \tag{3}$$

where we assume that the parameters μ and μ' take values in the interval [1, 4] (where the interesting behavior of this map takes place) and give rise to a coupling between the two variables. Therefore, μ and μ' depend on y_n and x_n, respectively. The simplest choice that satisfies these conditions is the linear one. Among the possible choices we analyze three couplings that lead to the following 2D maps

$$x_{n+1} = f_b(x_n, y_n) \qquad y_{n+1} = f_b(y_n, x_n) \tag{4}$$

where

$$\text{model (a)} \quad f_b(x_n, y_n) = b(3y_n + 1)x_n(1 - x_n) \tag{5}$$

$$\text{model (b)} \quad f_b(x_n, y_n) = b(3x_n + 1)y_n(1 - y_n) \tag{6}$$

$$\text{model (c)} \quad x_{n+1} = b(3y_n + 1)x_n(1 - x_n)$$

$$y_{n+1} = b(3x_{n+1} + 1)y_n(1 - y_n). \tag{7}$$

We add an adjustable parameter b in order to have different dynamical evolutions. The first two maps have a reflexion symmetry while the third includes a time asymmetric feedback. (We notice that a similar behavior can be obtained in two logistic maps with an additive (diffusive) coupling in some particular cases [7, 8].)

2.2. *Fixed points*

For the sake of convenience the fixed points are gathered in two groups

(1) On the axes

$$p_0 = (0, 0),\ p_1 = \left(\frac{b-1}{b}, 0\right),\ p_2 = \left(0, \frac{b-1}{b}\right). \tag{8}$$

(2) On the diagonal

$$p_{3,4} = \frac{1}{3}\left\{1 \mp \left(4 - \frac{3}{b}\right)^{1/2}, 1 \mp \left(4 - \frac{3}{b}\right)^{1/2}\right\}. \tag{9}$$

Points p_1 and p_2 are only fixed for models (a) and (c). The origin and those in group (2) are fixed in the three models. The stability of the two groups of points are analyzed separately, because they differ for the different models.

Group 1. (i) For $0 < b < 1$, p_0 is a sink and $p_{1,2}$ are hyperbolic points on the negative side of the axes. (ii) When $b = 1$, $p_0 = p_1 = p_2$. (iii) For $b > 1$, p_0 is a source point and $p_{1,2}$ are hyperbolic points, but now the positive side of the x-axis is the stable manifold of p_1 and the positive side of the y-axis the stable manifold of p_2.

Group 2. The stability of the points $p_{3,4}$ on the diagonal is more interesting. (i) For $0 < b < 3/4$, $p_{3,4}$ are not possible solutions. (ii) For $b = 3/4$, $p_3 = p_4$ is a unique stable point. (iii) For $3/4 < b < \sqrt{3}/2$, p_3 is an hyperbolic point. Its unstable direction coincides with the stable manifold of p_4, which is a sink in this interval. Therefore, the diagonal between p_3 and p_4 is a heteroclinic orbit. These three features are common for all the models (a)–(c), but the stability beyond these values are different. Therefore we present the results in two separated paragraphs.

2.3. *Bifurcations for models (a) and (b)*

When $b > \sqrt{3}/2$, p_4 destabilizes via a pitchfork bifurcation, becoming a hyperbolic point that splits into two points $p_{5,6}$

$$p_{5,6} = \left(\frac{2b(b+1) \mp \sqrt{b(b+1)(4b^2-3)}}{b(4b+3)}, \frac{2b(b+1) \pm \sqrt{b(b+1)(4b^2-3)}}{b(4b+3)}\right). \tag{10}$$

The difference between maps (a) and (b) is that there is a period 2 oscillation between points $p_{5,6}$ in the first case, while in the second there is a pitchfork bifurcation again, leading to p_5 or p_6 depending on the initial conditions. The location of points $p_{5,6}$ have been calculated using the reflection symmetry of the attractor. They always lie on a line parallel to the transversal diagonal.

The iterates begin to spiral around $p_{5,6}$ for $b = 0.956$. These spirals preclude the formation of the limit cycles around the fixed points $p_{5,6}$. The Hopf bifurcation occurs for $b = 0.957$. In the first model there is an alternation between the two limit cycles around p_5 and p_6 while only one of these cycles is visited by the map (6) depending on the initial point in the iterations. We gather the results for the limit cycles in these models for a higher values of b ($b = 1$). The situation differs in models (a) and (b). This is clear in Figs 1 and 2. These figures represent the iteration values after some time steps, the temporal spectrum and the values in the area $[0, 1] \times [0, 1]$ for model (a) and (b) respectively. (These figures have been obtained by taking 1.5×10^4 iterations, starting from an arbitrary initial point.) This is clear after looking at the spectra in Figs 1 and 2. In this situation the spectrum in Fig. 1 has different sharp peaks: one of high frequency ($w_1 = 0.5$) comes from

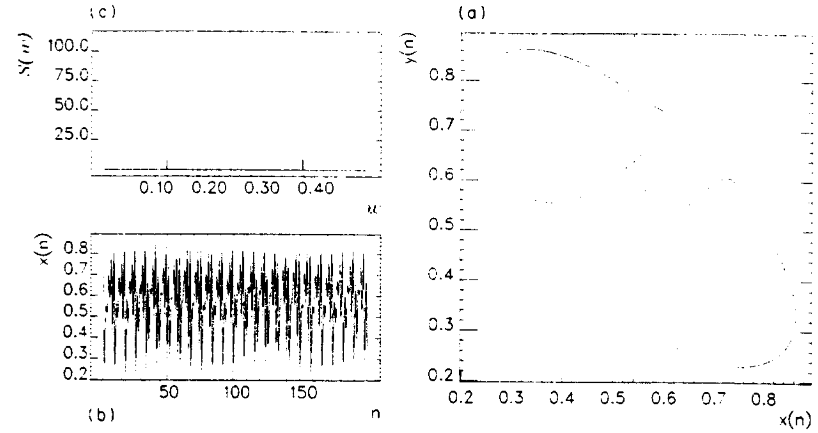

Fig. 1. (a) Iterates of *model (a)* [equation (5)] giving a couple of symmetric limit cycles for $b = 1$; (b) temporal signal x_n; (c) temporal spectrum of the signal.

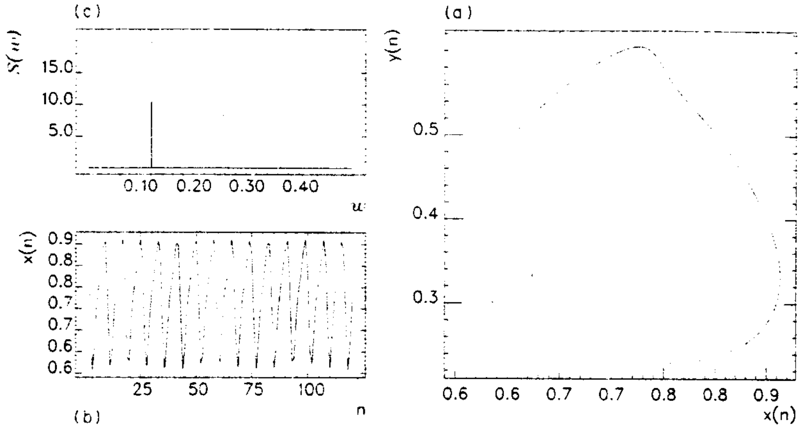

Fig. 2. (a) Iterates of *model (b)* [equation (6)] giving a single limit cycle $b = 1$; (b) temporal signal x_n; (c) temporal spectrum of the signal.

the alternation between the two limit cycles in the iteration process. A second one w_2 (which is b-dependent) is associated with the characteristic frequency of each cycle. The rest of the peaks correspond to the harmonics of w_2 and some combinations $|w_1 - nw_2|$ ($n = 1, 2, 3$). The spectrum of model (b), however only shows the frequency w_2 and its harmonics.

2.4. *Bifurcations for model (c)*

In model (c) the point p_4 is a stable sink until $b = 1$. For this value the point suffers a Hopf bifurcation and a limit cycle around p_4 appears. Figure 3 shows the iterates for

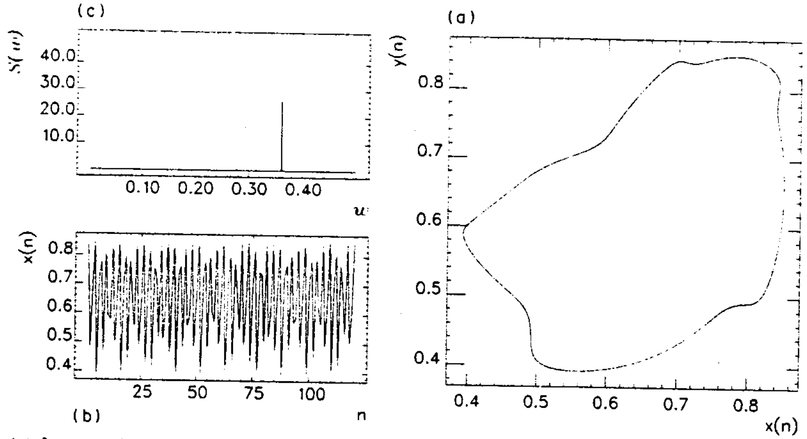

Fig. 3. (a) Iterates of *model (c)* [equation (7)] giving a limit cycle for $b = 1.096$; (b) temporal signal x_n; (c) temporal spectrum of the signal.

$b = 1.096$. For $1 < b < 1.18$ the limit cycle show some quantitative changes, because the spectrum always show some sharp peaks corresponding to quasiperiodic motions. In the spectra two peaks, both depending on b appear. (One is quite clear $w_3 = 0.36$, the second $w_4 = 0.08$ is very small in this scale.) For example, for $b = 1.12$ the unique limit cycles collapse into three islands, but without any sensitive change in the spectrum as one can see in Fig. 4. (One can appreciate two frequencies $w_4 \simeq 0.06$ and $w_3 \simeq 0.34$ and the combination $w_3 - w_4$.) For $b > 1.148$ the cycle is folded (see Fig. 5) with more harmonics (some of their peaks are very small) in the spectrum.

3. TRANSITION TO CHAOS

3.1. *Models (a) and (b)*

For b slightly larger than 1 the limit cycles approach the stable manifold of the hyperbolic point p_4 giving rise to a folding process. However, the system is still quasiperiodic in the case (a) and merely periodic in case (b). (This is given in Fig. 6 and 7 for $b = 1.03$.) When b reaches the value $b = 1.03$ the limit cycles can cross the stable manifold of p_4 that coincides with the heteroclinic orbit between p_0 and p_4 and some irregular motions appear around this point.

For $1.032 < b < 1.0843$ the limit cycles still grow and fold becoming very complex. A typical chaotic situation ($b = 1.070$) is given in Figs 8 and 9. The iterations in this range of b give rise to a interlacing of the two limit cycles on the diagonal and a complex folding process around the unstable upper fixed point p_4. In this region the w_1-frequency peak and its harmonics are slowed down to noisy bands in model (a) (Fig. 8). For both models a widening process of the w_2-peak and its harmonics appear, as can be seen in Figs 8 and 9. The complexity of the iterates is always localized around two regions: near p_4 and near the hyperbolic points $p_{1,2}$. However, the route to chaos is quasiperiodic for model (a) and monoperiodic in case (b). Spectra in Figs 8 and 9 ($b = 1.07$) reveal this important difference.

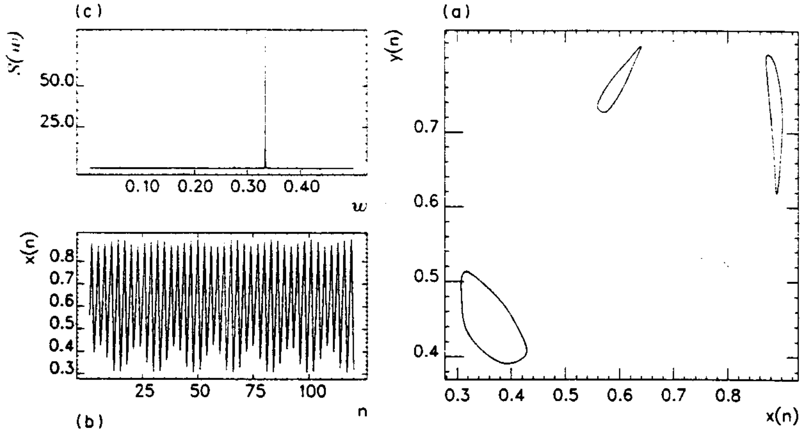

Fig. 4. (a) Collapse of the limit cycle in *model (c)* to three islands for $b = 1.12$; (b) iterations; (c) Fourier spectrum (arbitrary units).

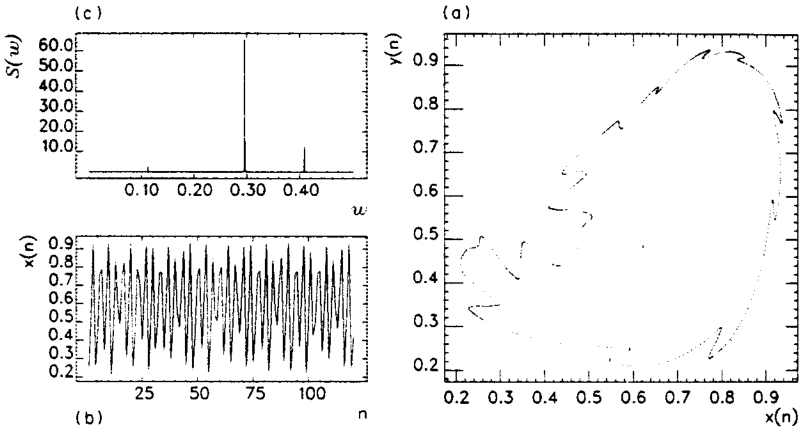

Fig. 5. (a) Folded attractor of *model (c)* for $b = 1.148$; (b) iterations; (c) spectrum.

Finally when the limit value $b = 1.084322$ is reached the attractor is tangent to its basin boundary and the iterates can cross the axes. They are attracted by the stable manifold (the axes) of the saddle points $p_{1,2}$, but when they arrive at the neighborhood of the unstable manifolds of these points they can escape to infinity and therefore the attractor is destroyed.

To confirm the characteristics of the observed bifurcations, the larger Lyapunov exponent λ is studied. (This has been calculated by the Jacobian standard method on 10^3 points of a trajectory [9].) Of course, some slight differences in the λ for the two models (a) and (b) exists. The result is given in Fig. 10. λ goes to zero when a bifurcation point is

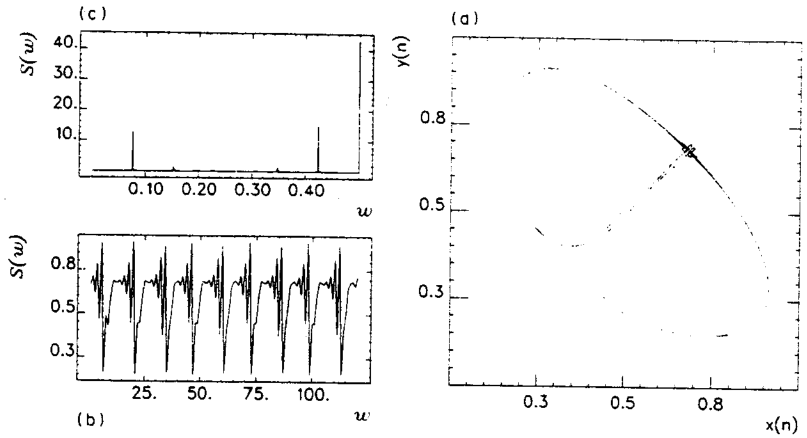

Fig. 6. (a) Folded limit cycles of *model (a)* for $b = 1.03$; (b) iterations (c) spectrum.

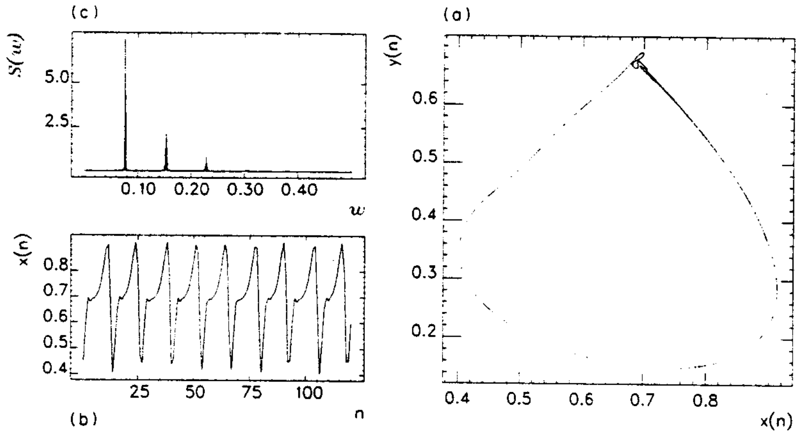

Fig. 7. (a) Folded limit cycle of *model (b)* for $b = 1.03$; (b) iterations; (c) spectrum.

approached. It also gives a zero value for the interval of b that corresponds to the appearance and development of the limit cycles. For some values of b, $\lambda < 0$ and only some points on the limit cycles are visited by the iterations (quasiperiodicity and periodicity, respectively). For the value $b = 1.025$, λ becomes positive in small intervals that alternate with periodic windows ($\lambda < 0$). But when $b = 1.032$, λ reaches a value that corresponds to the beginning of a chaotic band. From Fig. 10 one can also deduce the existence of periodic windows where $\lambda < 0$ in this range of b.

It is obvious that the properties of the two coupled maps is not a direct consequence of the properties of a single logistic. Its transition is reminiscent of the Ruelle–Takens type [9]

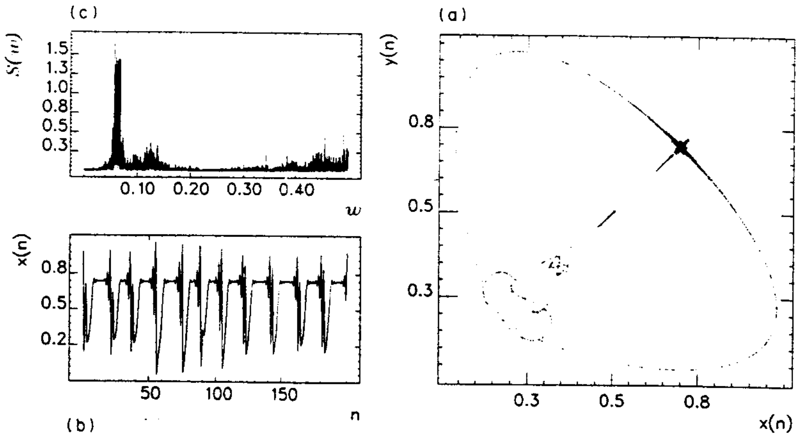

Fig. 8. (a) Chaotic attractors in *model (a)* for $b = 1.07$; (b) iterations; (c) spectrum.

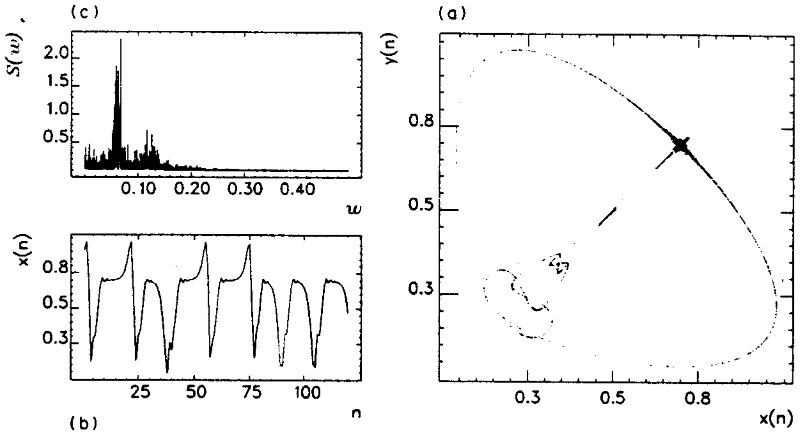

Fig. 9. (a) Chaotic attractor of *model (b)* for $b = 1.07$; (b) iterations; (c) notice that the spectrum differs from that in Fig. 8.

for the model (a). In model (b) the transition is precluded by only one frequency and, therefore is of Curry–Yorke type [9].

3.2. *Model (c)*

The transition to chaos in the model (c) is relatively more standard than in the preceding cases. The larger Lyapunov exponent in this case is given in Fig. 11. From this calculation it is clear than, apart from some chaotic bands ($b \simeq 1.14$, $b \simeq 1.155$) the folded limit cycle explodes into a chaotic attractor for $b = 1.17$. In Fig. 12 we show this attractor in the case of $b = 1.18$. One can see that it also resembles a part of the attractor of models (a) and

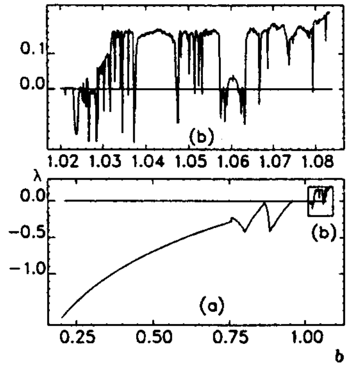

Fig. 10. (a) Largest Lyapunov exponent λ of model a as a function of the adjustable parameter b; (b) enlarged view of $\lambda(b)$ in the chaotic region.

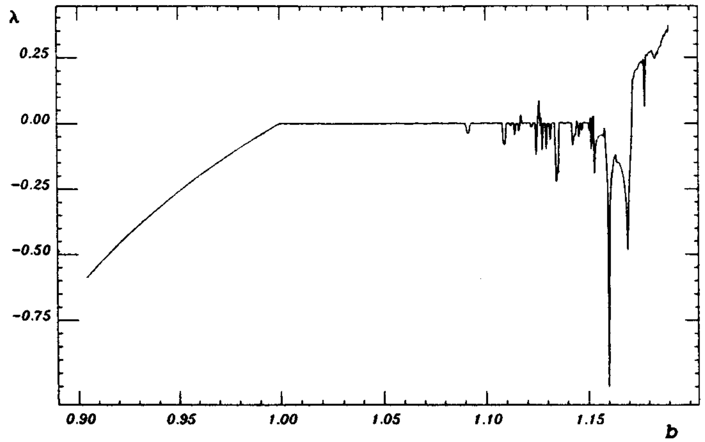

Fig. 11. Largest Lyapunov exponent λ of *model (c)* as a function of the adjustable parameter b.

(b). The spectrum shows clearly a sharp noisy band around the main frequency, but a band also appears at the frequency $w_1 = 1/2$ and near $w = 0$.

As this model shows a transition of the Ruelle–Takens type we do not give more details on the chaotic attractor.

3.3. *Universality class*

Models (a)–(c) correspond to couple two logistic maps with different couplings. We also tested with other maps of the same universality class. So, by following the ideas of Feigenbaum [10] we take different convex maps with one maximum only in the interval (0, 1). The maps analyzed are

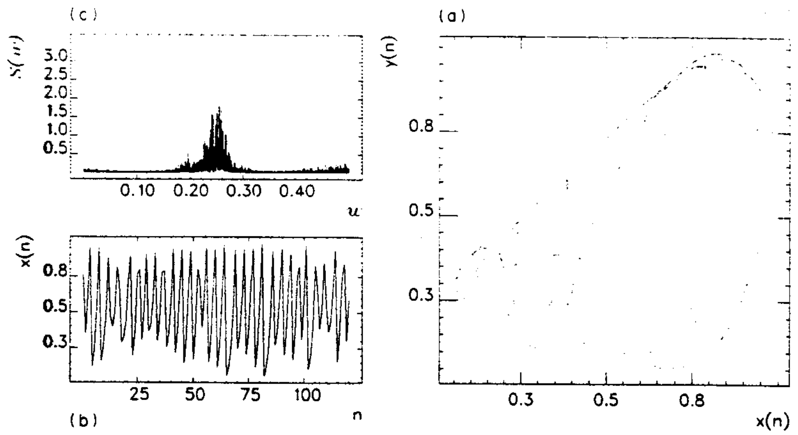

Fig. 12. (a) Chaotic attractors in *model (c)* for $b = 1.18$; (b) iterations; (c) spectrum.

$$\text{model (d)} \qquad f_b\,(x_n, y_n) = b\,\frac{(\pi - 1)}{\pi}\, y_{n+1} \sin(\pi x_n) \tag{11}$$

$$\text{model (e)} \qquad f_b\,(x_n, y_n) = b(\tfrac{27}{4}\, 3y_{n+1} + 1)x_n(1 - x_n)^2. \tag{12}$$

We repeated the analysis made with models (a)–(c). The main conclusion is that although some quantitative difference are obtained, the route to chaos is similar to that in models (a)–(c) based on the coupled logistic map. The transition is from fixed points to a period-2 orbit (alternation between two points), a Hopf bifurcation of the corresponding alternating points and, finally, a collision of the two orbits leading to chaos.

4. GLOBALLY COUPLED MAPS

In this section we consider the dynamics of an ensemble of maps globally coupled with a feedback. Following the analogy quoted in the Introduction we consider a global coupling between the single element and the henceforth modified background.

Kaneko [6, 7] has studied extensively the additive coupling among 1D maps given in equation (2). He discussed the different phases between a complete disordered phase and a coherent one [6, 7]. In a more recent paper he found that GCM systems, where the single element is in a chaotic regime violates the law of large numbers but not the central limit theorem [11]. Of course, this result is only partially surprising because correlations are not completely destroyed in a GCM system even in the disordered phase. In the simple case of diffusively coupled map lattices (CML) [equation (1)] the position of a given element does enter in the description. A 'correlation length' ξ can be defined in these CML, and the mutual information on the lattice must decrease as ξ/N, where N is the number of coupled elements.

In the case of globally coupled maps (GCM) [equation (2)] a correlation length does not exist because the coupling does not depend on the position. Therefore the mutual information in this case may not decay even for big values of N. However, the main conclusion of this paper seems to be that the feedback mechanism in GMC is sufficient to give a Gaussian distribution for the average, but the mean-square deviation of this average saturates with the number of elements in the ensemble N for $N < 10^4$. This is confirmed by looking at the spectrum of the time series that does not change for $N_c \simeq 10^4$ [11].

Here we analyze the case of a multiplicative global coupling, i.e. the 'mean field' is included in the multiplicative parameter b. The average of equation (2) must lead to a some kind of 'white noise' when the ensemble elements give random uncorrelated (zero coupling parameter) numbers, while in the same limit the 'noise' is 'multiplicative' in our system. As a consequence, possible advantages of the coupling considered here are: (a) that something more structured than a Gaussian distribution can be obtained for the average and (b) that the saturation value N_c is expected to be smaller than in the additive case, because a multiplicative coupling is more sensitive to changes in parameter space.

The analysis will be restricted to a generalization of the 2D map (5) to an N-dimensional case by the coupling

$$x^i_{n+1} = f_{b,N}(x^i_n, y^i_n) \qquad y^i_{n+1} = f_{b,N}(y^i_n, x^i_n) \tag{13}$$

with

$$f_{b,N}(x^i_n, y^i_n) = b\left[3\left(\frac{y^i_n + \varepsilon Y^N_n}{1 + \varepsilon}\right) + 1\right] x^i_n(1 - x^i_n) \tag{14}$$

being ε a coupling parameter and X^N_n and Y^N_n an average over the ensemble of elements

$$X^N_n = \frac{1}{N}\sum_{j=1}^{N} x^j_n. \tag{15}$$

The analysis is made by taking a fixed value of the parameter b ($b = 1.07$) in the chaotic region of the 2D map (see Fig. 8) recording the variations of one element of the coupled map and the average position for different values of the parameter ε and the number of elements N. Because of the complex coupling among the maps only a numerical study can be made. However, the random and coherent phases should be recovered in the limiting cases $\varepsilon = 0$ and $\varepsilon = \infty$, respectively.

Figure 13 shows the attractor of the iterates for a single element and for the average, for fixed ε ($\varepsilon = 0$) and two different N. The attractor of a single element and that of the average for $N = 100$ are given in part (a) and the corresponding spectra are given in (b) and (c), respectively. For $N = 1000$ the results are in Fig. 13 (d)–(f). Although the spatial distribution of the average in the plane is Gaussian-like, the spectrum shows some structure (the peaks are very small) due to the fact that we are not averaging uncorrelated values, but they are on a chaotic attractor. [See Fig. 13(b) and (e).]

More interesting is the case for a small ε ($\varepsilon = 0.01$) for different N. We observe that the feedback gives rise to the appearance of a peak with $w_1 = 1/2$, which is not present in the spectrum of model (5) for the same value of b (see Fig. 8). But for $N = 100$ the average is on a single cloud [Fig. 14(a)], while for $N = 1000$ it splits into two regions symmetric with respect to the diagonal [Fig. 14(d)]. The average in this situation leads to an enhancement of the peak $w_1 = 1/2$ in the spectrum of a single map. Therefore, contrary to the case of Kaneko, we observe here that the average is not on a single Gaussian-like distribution, but there is a period-2 that arises from the feedback mechanism as one can see in the spectrum of the average given in Fig. 14(f).

A very strange phenomenon is seen for $\varepsilon = 0.1$. The average shows a more detailed structure compared with smaller ε. The attractor of the single element and the 'attractor' of the average are very complex in space [Fig. 15(a)]. However the spectrum is clearly

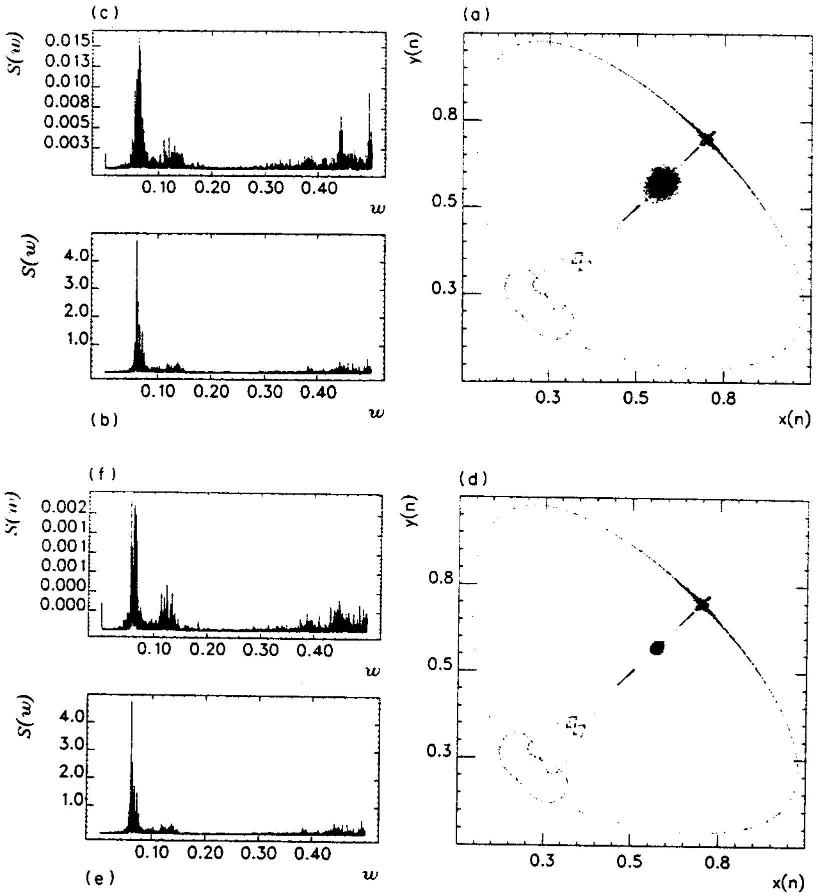

Fig. 13. Iterates of globally coupled map [equation (14)] for $\varepsilon = 0$ and $N = 100$: (a) iterates of a single element (chaotic attractor) and of the average (cloud of point in the center): (b) temporal Fourier spectrum of a single component (arbitrary units: notice that the height of the peaks do not coincide to that in Fig. 8 because less iterates are taken): (c) temporal Fourier spectrum for the average: (d)–(f) the same as (a)–(c) for $N = 1000$.

quasiperiodic. Therefore, a kind of synchronization through the feedback mechanism is established. And the feedback mechanism depends on N, as one can see by comparing Figs 15(a) and (d).

These features change for different values of ε and a monotonic behavior is not observed. For $\varepsilon = 1$ the results are very sensitive to the value of N. For $N = 100$ the attractors are quasiperiodic, both in space and time [Fig. 16(a)]. But for $N = 1000$ a broad dispersion of points (now the two attractor are mixed) in space and chaotic spectra with a broad peak near $w_1 = 1/2$ is obtained [Fig. 16(d)–(f)]. For higher values of ε ($\varepsilon = 10$) one has chaotic attractor for $N = 100$ (Fig. 17(a)–(c) and quasiperiodic ones for $N = 1000$ [Fig. 18(d)–(f)]. For the very strong coupling parameter $\varepsilon = 1000$ the attractors are chaotic and some small changes are observed when N is increased (Fig. 18).

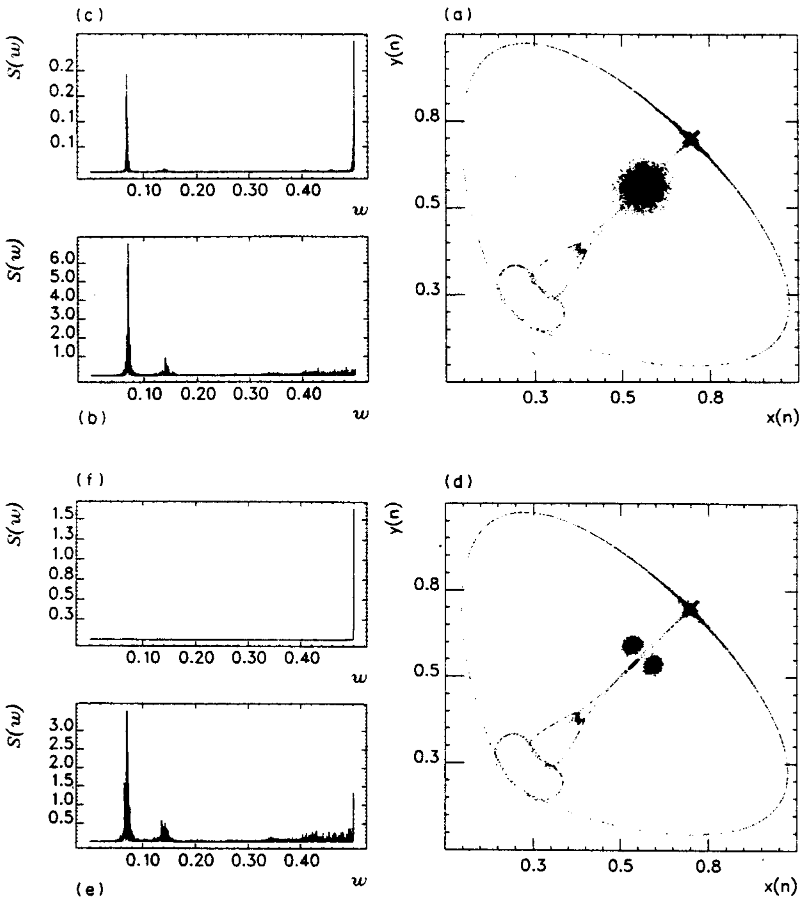

Fig. 14. Iterates of globally coupled map [equation (14)] for $\varepsilon = 0.01$ and $N = 100$: (a) iterates of of a single element and of the average: (b) temporal Fourier spectrum of a single component (arbitrary units:) (c) temporal Fourier spectrum for the average: (d)–(f) the same as (a)–(c) for $N = 1000$.

Let us summarize briefly the results in this section. The main conclusion is that a chaotic system with many elements coupled by a feedback can show very rich dynamics. Different behaviors are obtained depending on the values of the coupling parameter and the number of elements considered. In the numerical analysis of the system proposed in the present work one sees that (1) for a very small value of ε the feedback adds some kind of alternation; (2) the dynamics of the system and the average become synchronized for $\varepsilon = 0.1$ and (c) quasiperiodic or chaotic attractors are obtained depending on both ε and

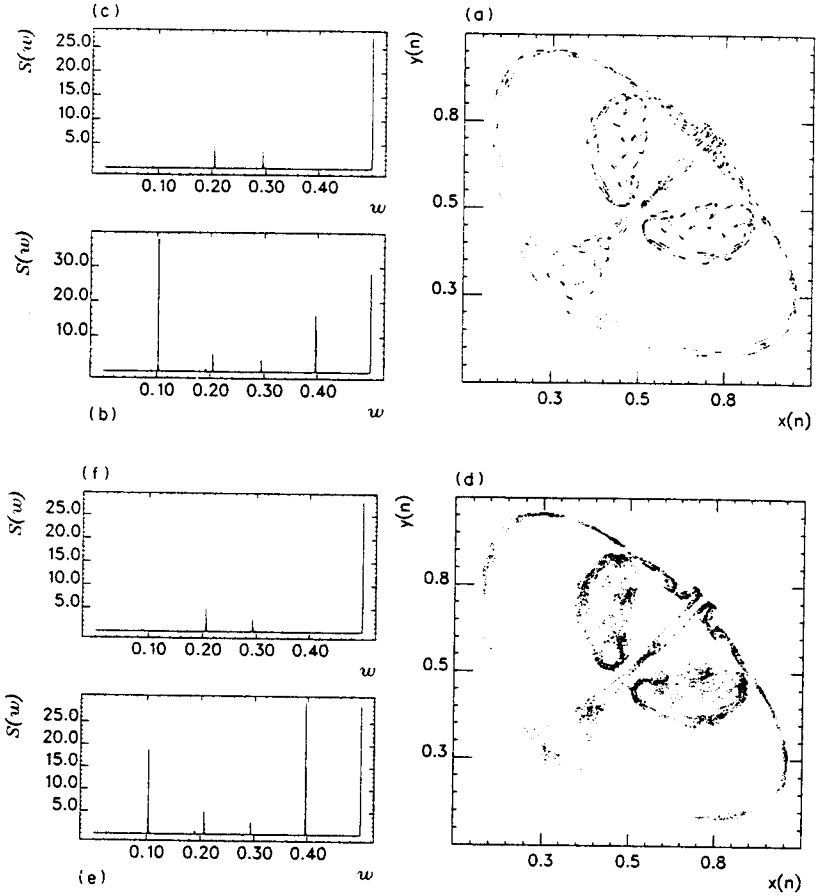

Fig. 15. Iterates of globally coupled map [equation (14)] for $\varepsilon = 0.1$ and $N = 100$: (a) iterates of of a single element and of the average; (b) temporal Fourier spectrum of a single component (arbitrary units); (c) temporal Fourier spectrum for the average; (d)–(f) the same as (a)–(c) for $N = 1000$.

N, but the behavior is not monotonic. (We intend to analyze in more detail this point in a future work.)

5. CONCLUSION AND DISCUSSION

We analyzed the role of a multiplicative coupling among maps. First we have shown that the dynamics of two maps with such a coupling cannot be reduced to that of the single element. The main result in this section is that one can obtain a transition to chaos in a 2D

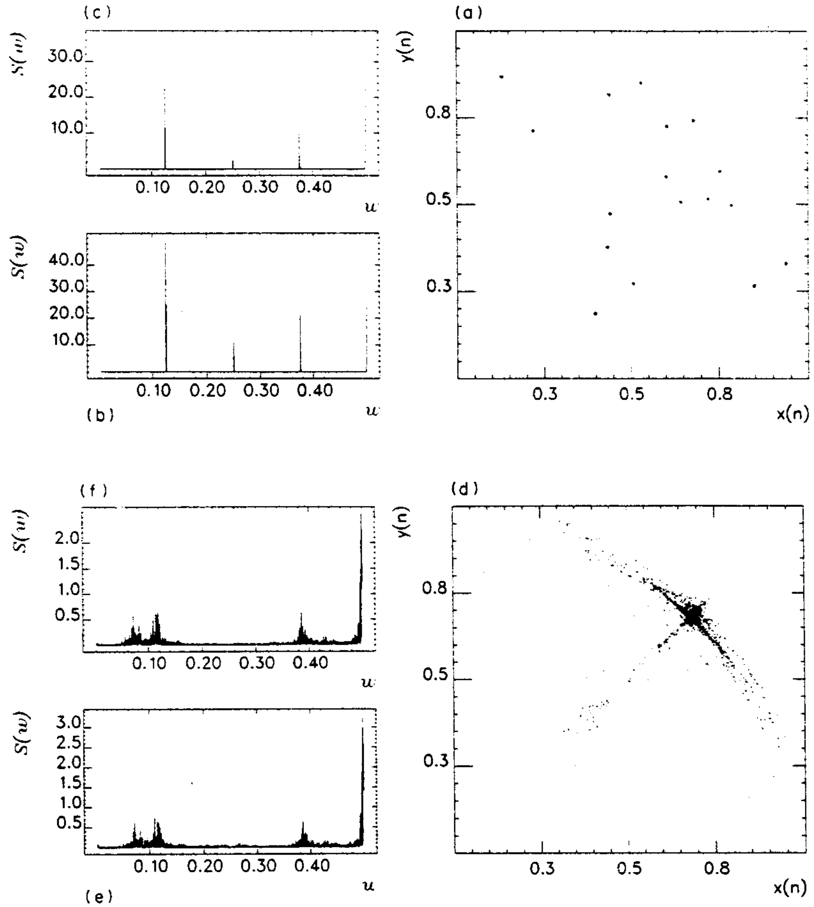

Fig. 16. Iterates of globally coupled map [equation (14)] for $\varepsilon = 1$ and $N = 100$; (a) iterates of of a single element and of the average; (b) temporal Fourier spectrum of a single component (arbitrary units); (c) temporal Fourier spectrum for the average; (d)–(f) the same as (a)–(c) for $N = 1000$.

discrete system precluded by only one frequency (model b) (Curry–Yorke type). In other cases the transition is equivalent to the Ruelle–Takens route [9].

But the results of global or multiplicative couplings must strongly differ when many maps interact. We have analyzed numerically this case for a particular model (a). This analysis shows that an ensemble of maps interacting globally by a multiplicative coupling can have many phases. Instead of giving the number of different clusters in the system [6, 7]. We studied global properties, i.e. the dynamics of one of the maps and the average. On one side the single map and the average behavior changes with the coupling strength ε and the number of maps N in a very complex manner. Depending on the values of these two

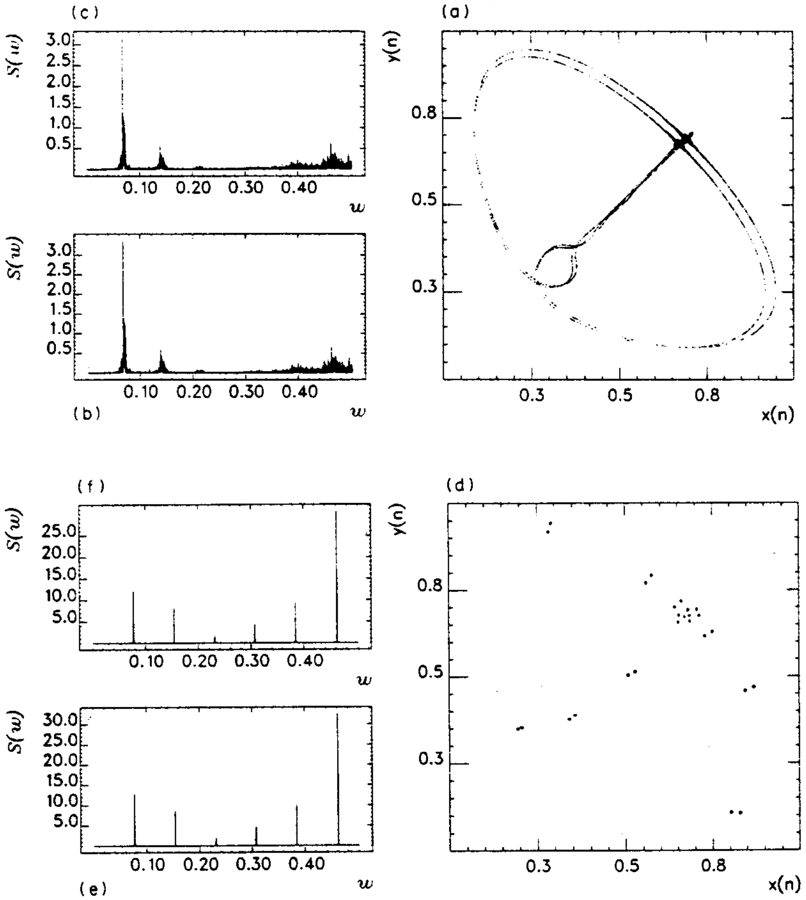

Fig. 17. Iterates of globally coupled map [equation (14)] for $\varepsilon = 10$ and $N = 100$: (a) iterates of of a single element and of the average; (b) temporal Fourier spectrum of a single component (arbitrary units); (c) temporal Fourier spectrum for the average; (d)–(f) the same as (a)–(c) for $N = 1000$.

parameters one can obtain a synchronization on a quasiperiodic or chaotic attractor, between the maps and the average, with very strange spatial behavior.

We think that these features can give some insight into the behavior of extended systems with many interacting modes, where only global properties can be measured.

Acknowledgements—We would like to acknowledge Dr M. Bestehorn (Stuttgart) for helpful comments and discussion. This work was supported by an EEC project SC1-0035-C and a DGICYT (Spanish Ministry of Education) project PB90-0362. One of us (R.L-R) acknowledges the Gobierno Foral de Navarra (Spain) for a research grant.

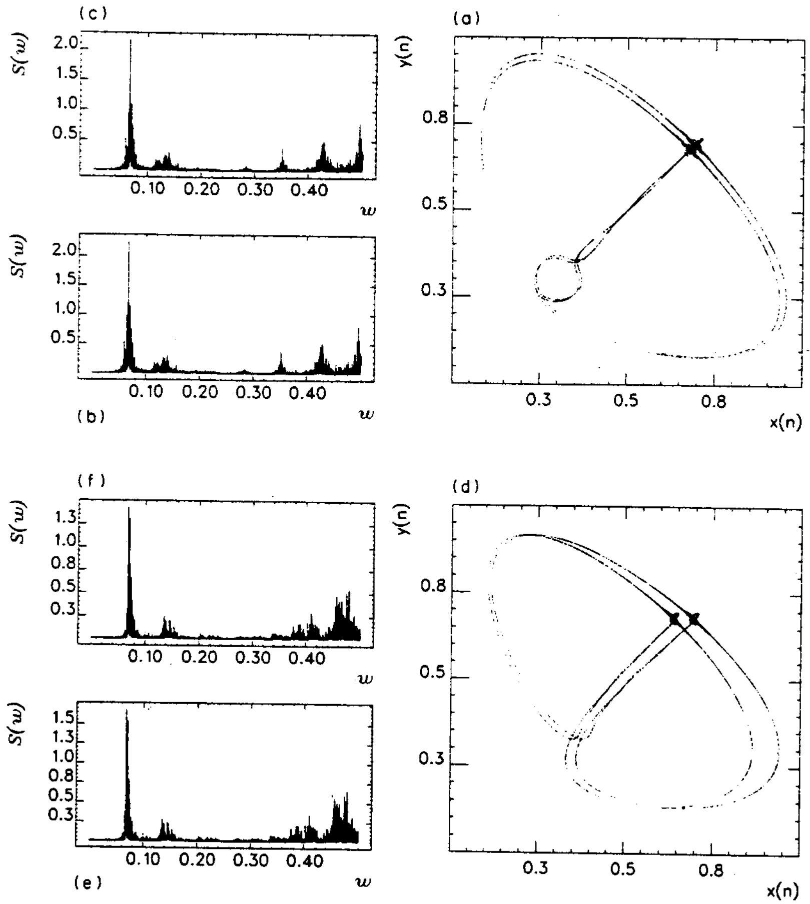

Fig. 18. Iterates of globally coupled map [equation (14)] for $\varepsilon = 1000$ and $N = 100$: (a) iterates of of a single element and of the average; (b) temporal Fourier spectrum of a single component (arbitrary units); (c) temporal Fourier spectrum for the average; (d)–(f) the same as (a)–(c) for $N = 1000$.

REFERENCES

1. A. R. Bishop, G. Grüner and B. Nicolaenko, Eds, in *Spatio-Temporal Coherence and Chaos in Physical Systems*, *Physica D* **23D**, Vol. 1–3, North Holland, New York (1986).
2. P. Grassberger, *Int. J. Theor. Phys.* **25**, 907 (1986).
3. S. Wolfram, in *Theory and Applications of Cellular Automata*. World Science, Singapore (1986).
4. K. Kaneko, *Prog. Theor. Phys.* **74** 1033 (1985); *Physica D*, **34**, 1 (1989).
5. H. Chaté and P. Manneville, *Physica D* **32**, 409 (1988); **37**, 33 (1989).
6. K. Kaneko, *Phys. Rev. Lett.* **63**, 219 (1989); *Physica D* **37**, 60 (1989); *Physica D* **41**, 137 (1990).
7. E. Atlee Jackson, in *Perspectives of Nonlinear Dynamics*, Vol II, Cambridge University Press, Cambridge (1990).

8. R. L. Schult, D. B. Creamer, F. S. Henyey and J. A. Wright, *Phys. Rev. A* **35**, 3115 (1987).
9. P. Bergé, Y. Pomeau and Ch. Vidal, in *L'Ordre dans le Chaos*. Hermann, Paris (1984).
10. M. Feigenbaum, *J. Stat. Phys.* **21**, 669 (1979).
11. K. Kaneko, *Phys. Rev. Lett.* **65**, 1391 (1990).